2019

Full Correlation in a Multiconfigurational Study of Bimetallic Clusters : Restricted Active Space Pair-Density Functional Theory Study of [2Fe-2S] Systems

Samuel J. Stoneburner
Messiah University, sstoneburner@messiah.edu

Davide Presti

Donald G. Truhlar

Laura Gagliardi

Full Correlation in a Multiconfigurational Study of Bimetallic Clusters: Restricted Active Space Pair-Density Functional Theory Study of [2Fe-2S] Systems

Davide Presti, Samuel J. Stoneburner, Donald G. Truhlar,* and Laura Gagliardi*

Department of Chemistry, Chemical Theory Center, and Minnesota Supercomputing Institute, University of Minnesota, 207 Pleasant Street SE, Minneapolis, MN 55455-0431, USA.

Abstract

Iron-sulfur clusters play a variety of important roles in protein chemistry, and understanding the energetics of their spin ladders is an important part of understanding these roles. Computational modeling can offer considerable insight into such problems; however, calculations performed thus far on systems with multiple transition metals have typically either been restricted to a single-configuration representation of the density, as in Kohn-Sham theory, or been limited to correlating excitations only within an active space, as in active-space self-consistent field methods. For greater reliability, a calculation should include full correlation, i.e., not only correlation internal to the active space but also external correlation, and it is desirable to combine this full electron correlation with a multiconfigurational representation of the wave function; but this has been impractical thus far. Here we present an affordable way to do that by using restricted-active-space pair-density functional theory. We show that with this method it is possible to compute the entire spin ladder for systems containing two Fe centers bridged by two S atoms. On the other hand, with second-order perturbation theory only the high-spin states can be computed. A key result is that, in agreement with some experiments, we find a high-spin ground state for a relaxed reduced $[Fe_2S_2(SCH_3)_4]^{3-}$ cluster, which is a novel result in computational studies.

1. Introduction

Iron-sulfur (Fe-S) compounds are widely studied because of their key role in biochemistry;[1] Fe-S clusters are the prosthetic groups in many metalloproteins, such as ferredoxins, hydrogenase, NADH-dehydrogenase, and nitrogenase,[1–5] and they have significant roles involving electron transport in the metabolic pathways for both prokaryotic and eukaryotic cells.[6,7] Furthermore, Fe-S clusters are protagonists of the so-called "iron-sulfur world";[8–11] prebiotic Fe-S clusters containing organic linkers (such as glutathione[12] and other analogs, mostly thiolates[12,13]) have been demonstrated to be able to form in extreme conditions, and their formation has been shown to benefit from the presence of the UV-light radiation (i.e. photo oxidizing/photolytic environment) provided by the "young Sun".[12] This may have led to the formation of more complex Fe-S-based prebiotic molecules capable of organizing themselves into peptides, enzymes, and proteins.

In the present work, we consider a particular class of Fe-S clusters: those containing two Fe centers bridged by two S atoms (referred to as [2Fe-2S] for convenience); these clusters present an intermediate situation between the single-center Fe clusters, from which they are formed, and the three- and four-center Fe clusters which, together with [2Fe-2S], are involved in the formation of peptides. Their UV-light-driven synthesis, mentioned above, was elegantly described in a recent experimental paper.[12] Experimentally [2Fe-2S] clusters have been characterized extensively with UV-Visible optical absorption spectra, Mössbauer spectra, and EPR spectroscopy.[4,7,12–15] However, a direct assignment of low-lying electronic states is still unattainable in larger systems.[16] Theoretical studies have contributed significantly to the understanding of their electronic structure,[16–26] but as pointed out in the work of Sharma et al.,[16] the theoretical models adopted until recently are not straightforward and have given conflicting answers to key questions. Sharma et al.[16] pointed out the possibility that one could obtain more definitive results by using *ab initio* calculations free of the assumptions in a phenomenological model, in particular avoiding use of the Heisenberg double-exchange model.

Complexes containing transition metals, especially multiple transition metal atoms, frequently have intrinsically multi-configurational character, i.e., they cannot be well described by a single config-

uration state function (CSF). This characteristic is often called “static correlation” or “strong correlation”, and the work of Sharma et al.[16] featured a thorough treatment of the static correlation of iron-sulfur systems. However, in order to make comparisons with experiment, it is also important to treat dynamic correlation at a high level. Dynamic correlation represents a relatively small part of the total electronic energy, but it is often of utmost importance in quantitatively determining relative energies such as the energy ordering of different electronic states.

Kohn-Sham density functional theory (KS-DFT) in principle includes the full correlation energy (static and dynamic) without separating them; however, the available density functionals treat the correlation energy better in systems well described by a single configuration state function, probably because KS-DFT is based on a single-configuration representation of the electron density. Nevertheless it is often the best theory available and is therefore widely used for these systems.[17–23] Recent applications using extended broken-symmetry (EBS) KS-DFT[27] and variational Monte-Carlo[28] were used to obtain a reasonable ground-state relaxed geometry for these compounds.

Multi-configuration wave function methods have also been employed,[21,22] and they represent an attempt to overcome the limitation of single-CSF methods. Examples of multiconfiguration wave function methods include multiconfiguration self-consistent-field (MCSCF) methods such as the complete-active-space self-consistent-field method (CASSCF),[29] multi-reference configuration-interaction (MRCI) based on an MCSCF or CASSCF reference function,[30] and multi-reference second order perturbation theory (MRPT2) such as complete active space perturbation theory[31–33] (CASPT2). CASSCF involves full configuration interaction (full CI) in an active space, which can provide only a qualitatively correct description of the electronic wave function. The included correlation, that which is representable internal to the active space, consists of the static correlation and a small portion of the dynamic correlation; the remaining dynamic correlation, involving excitations into the virtual space, is the external correlation; CASSCF lacks most of the dynamic correlation because excitations to generate the electronic configurations are limited to the active space, which has a limited number of orbitals. The external correlation is usually treated by a post-SCF method, using the SCF orbitals to build a reference wave

function. When the reference wave function is multi-configurational, the method is called a multireference method. MRCI treats the full electron correlation when including sufficiently high excitations into the virtual space, but that is prohibitively expensive in most cases, so excitations are usually limited to single and double excitations (MRCISD). CASPT2 is also limited to double excitations in the virtual space, and although it is less expensive than MRCISD, it too is usually too expensive for large or complex systems.

In a recent work,[16,25] state-of-the-art methods for the treatment of large active spaces, e.g., the density-matrix renormalization group (DMRG) as a solver for complete active-space configuration interaction (CASCI), were employed by Sharma et al.[16] to explore the spin-ladder of the low-energy spectrum of [2Fe-2S] and [4Fe-4S] clusters; this allowed the use of larger active spaces than are practical for conventional CASSCF. But even with the largest practical active spaces, a large fraction of the dynamic correlation energy is missing in CASSCF.

While there have been many theoretical studies, to the best of our knowledge no one has yet treated these iron-sulfur clusters with conventional post-MCSCF dynamic correlation treatments such as MRCI or CASPT2. The lack of such applications to [2Fe-2S] clusters is due to their high or impractical cost. While the time required for an MRPT2 calculation can be reduced with the use of a parallelized code, the amount of memory becomes prohibitive for calculations involving the number of CSFs that would typically be required to calculate low-spin states involving transition metal compounds.

The objective of the present work is to combine the advantages of a multi-configurational representation of the density with an affordable treatment of the full correlation energy. We do this by using multi-configuration pair-density functional theory (MC-PDFT),[34] which evaluates an on-top density functional using the density and on-top pair density of a multi-configurational wave function. Unlike the energy calculation in MRPT2, where correlation energy is separated into an internal part treated by MCSCF and an external part involving a perturbative treatment of excitations into the virtual space, with MC-PDFT one computes the unpartitioned (i.e., full) electron correlation energy in a single step by using the multiconfigurational kinetic energy, density, and on-top pair density and an on-top density

functional. Only kinetic energy and classical Coulomb contributions are taken from the MCSCF wave function; the MCSCF energy is not used. Therefore there is no double counting of the correlation energy contribution to the electron-electron repulsion.[34–38]

In the present work we calculated the low-energy spin ladder for both oxidized and reduced [2Fe-2S] clusters and compared the results to literature data. The computational capabilities of MC-PDFT are illustrated for large active space with 22 electrons in 26 orbitals, giving rise, for example, to 6.3×10^6 CSFs for the triplet spin configuration. We achieve this larger number of CSFs by using a recently developed protocol, RASCI-PDFT,[39] based on the restricted active space self-consistent-field (RASSCF)[40]/configuration interaction (RASCI)[41] method. For comparison, RASCI-PT2[42] energies were computed whenever possible, but they were unaffordable except for a few cases; this shows that RASCI-PDFT can handle problems larger than those feasible with previously available post-MCSCF methods.

2. Computational Methods

All calculations were performed for gas-phase species using a parallel build of *Molcas 8.2*.[43] Symmetry constraints were not imposed. The ANO-RCC-VTZP large basis-set[44] was used for iron and sulfur atoms, and the ANO-RCC-MB minimal basis-set[44] was used for C and H atoms of the ligands. The Douglas-Kroll-Hess Hamiltonian[45–47] was employed throughout to account for scalar relativistic effects.

In the wave function calculations, external correlation was included perturbatively with the zero-order wave function obtained by RASSCF[40] and RASCI[41] (see Sections 2.2.1 and 2.2.2 for further details) by using second-order perturbation theory (to be indicated as RASCI-PT2). RASSCF calculations involve simultaneous optimization of both orbitals and configuration interaction coefficients. In the present RASCI calculations, the orbitals optimized by RASSCF for the high-spin configuration are used for restricted-active-space configuration interaction calculations for the whole spin-ladder. The active spaces employed are described in detail in the next section. RASSCF and RASCI excitation energies were

computed with the state-average[48] (SA) approach. RASCI-PT2 calculations were carried out as single-state calculations (based on state-averaged orbitals) with an imaginary shift[49] of 0.1 hartrees and with the default value (0.25 hartrees) for the IPEA shift.[50] For spin multiplicity M (which equals $2S + 1$, where S is the total electron spin) lower than 8, memory allocation for MRPT2 calculations exceeded the maximum available for our hardware, thus rendering the calculations unfeasible.

The density functional calculations are carried out with pair-density functional theory[34,51] based on RASCI wave functions and therefore are called RASCI-PDFT. The RASCI-PDFT calculations used the translated PBE (tPBE) on-top functional.[34]

Orbitals are depicted with a surface isodensity value of 0.4 a.u. Plots and figures were produced with *Gnuplot 5.0*, *Luscus,*[52] and *Vesta.*[53]

2.1 Cluster Models

We write superscripts $\pm q$ for chemical oxidation states, and superscripts $q\pm$ for physical charges. The central fragment of the compounds investigated here are the oxidized cluster $[2Fe\text{-}2S]^{2+}$, where both metal centers are formally in the oxidation state Fe^{+3}, and the reduced cluster is $[2Fe\text{-}2S]^{1+}$, where one center is Fe^{+3}, and the other one is Fe^{+2}. The oxidized cluster has ten unpaired electrons in the high-spin (HS) configuration, and the reduced cluster has nine. Since [2Fe-2S] clusters have four thiolate linkers, the full systems under study (shown in Figure 1) are denoted as $[Fe_2S_2(SCH_3)_4]^{2-/3-}$. The unrelaxed structures from Sharma et al.[16] were used for both the oxidized and reduced forms. For the reduced cluster, $Fe_2S_2(SCH_3)_4]^{3-}$, the slightly asymmetric relaxed structure, obtained by broken-symmetry KS-DFT and reported in Ref. 16, was also considered.

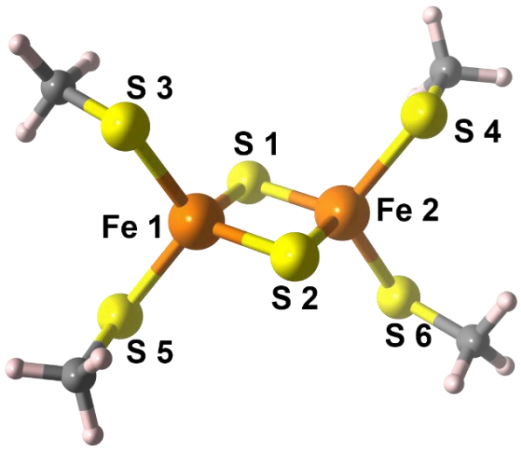

Figure 1: Unrelaxed structure and atom labeling of the $[Fe_2S_2(SCH_3)_4]^{2-/3-}$ cluster as taken from Ref. 16 (derived, in turn, from the experimental structure of Ref. 54)

2.2. Active space determination

2.2.1 RASSCF

The active spaces used in the present study are defined based on the ones reported in Ref. 16. The high-spin (HS) spin state of the $[Fe_2S_2(SCH_3)_4]^{2-}$ oxidized cluster (M = 11) was used to generate the active spaces used for both oxidized $[Fe_2S_2(SCH_3)_4]^{2-}$ and reduced $[Fe_2S_2(SCH_3)_4]^{3-}$ clusters. See the SI for details of the protocol. While it is possible that the use of orbitals optimized only for high-spin when calculating the full spin ladder could introduce some bias favoring higher spin states, we note that the DMRG calculations in Ref. 16 also used orbitals optimized for a high-spin state. After a comparison with results from orbitals optimized for each spin state, the authors concluded that the effect on relative spin energetics was minimal and performed CI-only calculations with the high-spin orbitals thereafter.

The active spaces in RASSCF and RASCI calculations are labeled as (n,e,h;o_1,o_2,o_3), with n being the total number of electrons considered in the RAS1, RAS2, and RAS3 subspaces, e being the maximum number of electrons allowed to be excited from RAS1, h being the maximum number of holes allowed in RAS3, and o_1, o_2, and o_3 being the number of orbitals in RAS1, RAS2, and RAS3, respectively. The active spaces we use are explained in Table 1. The orbitals in the active spaces for the oxidized

case are depicted in Figure S2, and those for the reduced case are in Figures S3 and S4. (Figures and tables with a prefix S are in Supporting Information.)

Table 1. Active spaces employed in this work[a]

Cluster	Name	*n,e,h; o₁,o₂,o₃*	Description of orbitals
either	all		RAS1: bridging sulfur 3*p* orbitals RAS2: all 3*d* orbitals
oxidized	(22,26)	22,1,1; 6,10,10	RAS3: all 3*d*′ [b] orbitals (correlating orbitals)
	(22,21)	22,1,1; 6,10,5	RAS3: five 3*d*′ [b] orbitals with highest occupation numbers
reduced	(23,26)	23,1,1; 6,10,10	same as (22,26)
	(23,22)	23,1,1; 6,10,6	RAS3: six 3*d*′ [b] orbitals with highest occupation numbers (unrelaxed geometry)
	(23,21)	23,1,1; 6,10,5	RAS3: five 3*d*′ [b] orbitals with highest occupation numbers (relaxed geometry)

[a]In all cases, these orbitals were obtained by a state-averaged RASSCF calculation on the lowest ten roots of the high-spin cluster (multiplicity $M = 11$ for the oxidized; multiplicity $M = 10$ for the reduced). In the reduced case, the orbitals of the oxidized case are used as starting orbitals for the SCF iterations.
[b]The orbitals labeled 3*d*′ are a second subshell of d orbitals that contribute to the correlation of the first subshell of d orbitals; they are sometimes referred to as "4*d*" or "4*d*-like".

2.2.2 RASCI

Having obtained the orbitals by RASSCF calculations on the high-spin states, we performed RASCI calculations for the full spin ladder of each cluster; these calculations consisted of reoptimizing only the CI coefficients for every possible spin multiplicity using the orbitals optimized for the high-spin states of the cluster. The RASCI wave functions were also used as references for further calculations by MC-PDFT and MRPT2, and these calculations are labeled as RASCI-PDFT and RASCI-PT2, respectively. The RASCI energies without either MC-PDFT or MRPT2 are labeled simply "RASCI".

Since the number of CSFs grows rapidly with active space size (see Table 2), and since the RAS2 subspace already has 10 electrons in 10 orbitals, double excitations between RAS subspaces would have resulted in unaffordably large calculations for all spin multiplicities other than the highest-spin configurations ($M = 11$ for the oxidized cluster and $M = 10$ for the reduced cluster). We gauged the error in

RASCI excitation energies due to the use of single excitations between subspaces by also considering two holes in RAS1 for the high-spin configuration, while keeping only single excitations to RAS3 to limit the number of CSFs. We report in Table S1 the difference between the excitation energies obtained for the unrelaxed oxidized and reduced clusters with two holes or one hole allowed in RAS1. The mean differences are in the range -0.03 to 0.19 eV with the chosen active spaces.

Table 2. Number of configuration state functions (CSFs) for each spin configuration with 26 orbitals.

oxidized		reduced	
M	CSFs	*M*	CSFs
11	6,221	10	28,880
9	134,739	8	378,280
7	1,067,605	6	2,012,780
5	3,790,875	4	4,950,990
3	6,260,760†	2	5,241,060
1	3,409,164		

† This active space for the triplet state has 2.25 times more CSFs than the generalized active space (GAS)-PDFT calculation for triplet dodecacene that included 50 electrons in 50 orbitals.[55]

Many of the *3p* orbitals of bridging sulfurs are mixed with S–CH_3 σ-type bonding orbitals, especially in the case of the reduced cluster, and this makes the active spaces including 26 orbitals comparable to the large one with 32 orbitals employed in Ref. 16. The main remaining difference is that in this work the 4*s* orbitals of Fe were excluded because of their being highly mixed with 4*d* and 5*d* orbitals, which would have required several additional correlating orbitals in the active space in order to maintain balance. Furthermore, here the large ANO-RCC-VTZP basis-set is used (with ANO-RCC-MB for C and H), whereas the orbitals of Ref. 16 were obtained by a small basis set in BP86/def2-SV(P) calculations. Note that both our orbitals and those in Ref. 16 were optimized for a high-spin state, as stated in Section 2.2.1.

3. Results and Discussion

3.1 $[Fe_2S_2(SCH_3)_4]^{2-}$ oxidized cluster

The oxidized cluster has two centers that are formally Fe^{+3} centers; thus each of these centers has five unpaired electrons. The centers are antiferromagnetically (AFM) coupled[14] in the ground state of the oxidized cluster. The AFM state is an overall singlet, whereas the ferromagnetically (FM) coupled undectet is the highest spin state. We remind the reader that the orbitals are optimized with the FM configuration due to the significantly smaller number of configurations (see Table 2) in that spin state, and that the authors of Ref. 16 found little benefit in optimizing the orbitals for each spin state separately. Figure 2a shows the RASCI spin ladders for vertical excitation energies using both the (22,26) and the (22,21) active spaces. Energies are reported in the text in eV units for easier readability, whereas they are plotted in figures in cm^{-1} for easier comparison with Ref. 16. Note that 1 eV = 8065.5 cm^{-1}.

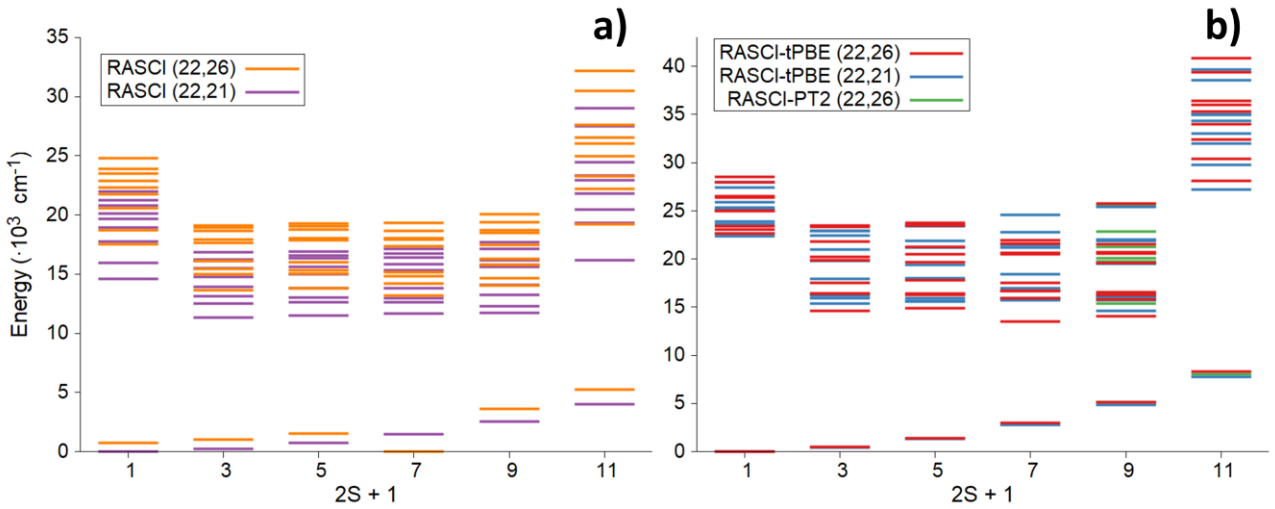

Figure 2. Vertical-excitation spin ladders. (a) RASCI (ten roots for each spin configuration) computed with two active spaces: (22,26) and (22,21). (b) RASCI-PDFT and RASCI-PT2 (nonet and undectet ground-state only). The singlet ground state is taken as the zero of energy in this figure, and for a visual comparison of excitations energies, the energy of the RASCI-PT2 nonet ground state is shifted to the energy of the RASCI-PDFT nonet ground state. In the figure, RASCI-PDFT is labeled RASCI-tPBE.

There is no tabulated data in Ref. 16 for the oxidized clusters, but Figure 2 therein depicts the ground-state energy levels for each spin state of the oxidized cluster. The DMRG-CASCI values in Ref. 16 span a larger range (approximately 8,000 cm^{-1}) than present RASCI calculations (about 5,000 cm^{-1} in Figure 2a), but it is difficult to say which results are more accurate. While the DMRG-CASCI calculation of Ref. 16 includes more orbitals in the active space (specifically, the 4*s* subshells of the Fe atoms) and a more complete treatment of the active space, a much larger basis set is adopted for the present work. Note that both the DMRG-CI and our RASCI calculations used orbitals optimized for the high-spin configuration, and therefore the differences in results cannot be explained by a possible high-spin bias in the orbitals. Figure 2a of the present work shows a sizable gap between the ground and the first excited states for all spin states, while the higher excited states form a denser manifold. We will see below that this trend is also found in post-RASCI energies computed by RASCI-PDFT and RASCI-PT2. Figs. 2a and 2b have slightly different wavenumber scales, but comparison of numerical relative energies shows that RASCI-PDFT has a mildly wider spread of excitation energies than does RASCI.

RASCI (22,21) energies give a trend that is comparable with RASCI (22,26), but while RASCI (22,26) incorrectly predicts the lowest energy spin state to be a septet, RASCI (22,21) correctly orders the different spin states increasing from singlet to undectet, as has been inferred from experiment. Although the RASCI calculation without external correlation does not obtain correct spin state order with the largest active space (i.e. including some but not all 3*d'* orbitals), Figure 2b shows encouragingly that RASCI-PDFT does yield the correct spin state ordering for the largest active space. Furthermore, for each spin state, the lowest states for each of the spins are almost superimposed in the RASCI-PDFT calculations, showing that RASCI-PDFT is less sensitive to active space choice than is RASCI. Notice that

For comparison, single-state RASCI-PT2 are reported only for the states for which there are converged results (the undectet ground state and the nonet ground and excited states), i.e., $M = 9$ and $M = 11$.

3.2 $[Fe_2S_2(SCH_3)_4]^{3-}$ reduced cluster

Calculations for the reduced cluster are reported at two geometries: the unrelaxed one (discussed in Section 3.2.1), which is the same slightly asymmetric structure as was used for the oxidized cluster, and the relaxed one (discussed in Section 3.2.2), which is more asymmetric. Both structures are from Ref. 16. Table 3 summarizes the vertical excitation energies of the lowest five electronic states (which are supposed to be more relevant experimentally at room temperature) for each spin configuration by RASCI, and compared to the DMRG-CASCI results of Sharma et al.[16]

The work of Sharma et al. involved using the DMRG solver for CASCI with very large active spaces. Since CASSCF, even with a large active space, does not include most of the dynamic correlation, it is comparable to our RASCI in that neither calculation includes external correlation, whereas our RASCI-PDFT calculation includes dynamic correlation with no active space limitation. However, the DMRG-CASCI provides an approximation to full CI within the active space, whereas our calculations involve restricted CI as explained in Section 2.2.1. Conversely, the basis set used for DMRG-CASCI was unusually small [def2-SV(P)] for a wave function calculation, whereas we use an extended basis set. Taking all of these factors into account, we cannot say definitively which set of results is more accurate, because we lack an external reference by which to judge between them, and the different approaches each have advantages and disadvantages in terms of the severity of their approximations.

3.2.1 Reduced cluster with unrelaxed geometry

The present RASCI calculations with the (23,22) active space on the unrelaxed geometry are not expected to capture most of the dynamic correlation due to the limitations of the active space, i.e., the number of orbitals as well as the restriction to having only single excitations from RAS1 and to RAS3.

Table 3 RASCI vertical excitation energies for the lowest five electronic states with respect to the DMRG-CASCI results of Sharma et al.[16] for the unrelaxed geometry of the reduced cluster. The lowest energies in each case are used as the zeroes of energy.

Excitation energies (eV)										
	RASCI (23,1,1;6,10,10)					**RASCI (23,1,1;6,10,6)**				
2S+1	**State 1**	**State 2**	**State 3**	**State 4**	**State 5**	**State 1**	**State 2**	**State 3**	**State 4**	**State 5**
2	0.07	0.24	0.40	0.47	0.53	1.27	1.46	1.74	1.96	2.16
4	0.04	0.31	0.35	0.46	0.62	1.24	1.62	1.67	2.12	2.13
6	0.07	0.21	0.34	0.64	0.72	1.24	1.62	1.83	2.15	2.29
8	0.09	0.17	0.37	0.87	0.95	1.30	1.60	2.08	2.23	2.34
10	0.00	0.34	0.50	1.14	1.24	0.00	0.31	0.33	0.98	1.13
	DMRG-CASCI, Sharma et al.[16]									
	State 1	**State 2**	**State 3**	**State 4**	**State 5**					
2	0.00	0.04	0.14	0.33	0.53					
4	0.02	0.07	0.21	0.53	0.55					
6	0.04	0.08	0.36	0.58	0.66					
8	0.08	0.16	0.58	0.67	0.79					
10	0.13	0.36	0.91	0.92	1.05					

Table 3 and Figures 3a and 3c show that the larger active space (23,26) yields results more similar to the DMRG-CASCI results than the smaller (23,22) active space in terms of vertical excitation energies, although the differences are still sizable. These differences cannot be simply explained with the choice of employing the orbitals optimized only for the dectet spin state, as the DMRG-CASCI used high-spin orbitals as well.[16] While the RASCI calculations present a different energetic ordering of the ground state of each spin state with respect to DMRG-CASCI, the ordering at the RASCI-tPBE level with the (23,26) active space is similar to the DMRG-CASCI results (see Table S3 and Figure 3d).

The (23,26) active space captures additional dynamic correlation even at the RASCI level due to the inclusion of all the correlating 3*d*´ orbitals of iron, which have previously been found to be important in first-transition-row metals with more than half-filled 3*d* subshells.[33,56,57] Also, the RASCI excitation energies (Figures 3a and 3c) and their spacings, i.e., both the global energy span and the spacings within each multiplet manifold, are more similar to those computed by DMRG-CASCI than was the case for the (23,22) active space.

When approximating the full correlation energy by RASCI-PDFT (Figure 3d), the situation does not change considerably. The finding that there are only small differences between the (23,26) active space and the active space of Sharma et al. indicates that the inclusion of the 4*s* orbitals (part of the so-called 'double-shell' effect, together with 3*d'* orbitals) in the active space is unneeded, as already reported in similar cases.[56,57]

The cluster is predicted by RASCI-PDFT to have a quartet ground state (Figure 3d) that is only 0.01 eV more stable than the doublet (see Table S3). As seen in the next subsection, this occurs for the relaxed structure as well. Note that we choose the doublet as the reference energy (zero of energy) in Table 3 and in Figure 3 (excepting Figure 3b), but the 0.01 eV is a small difference and below the expected precision of the method, thus we cannot make a reliable claim regarding whether the doublet or the quartet is the true ground state.

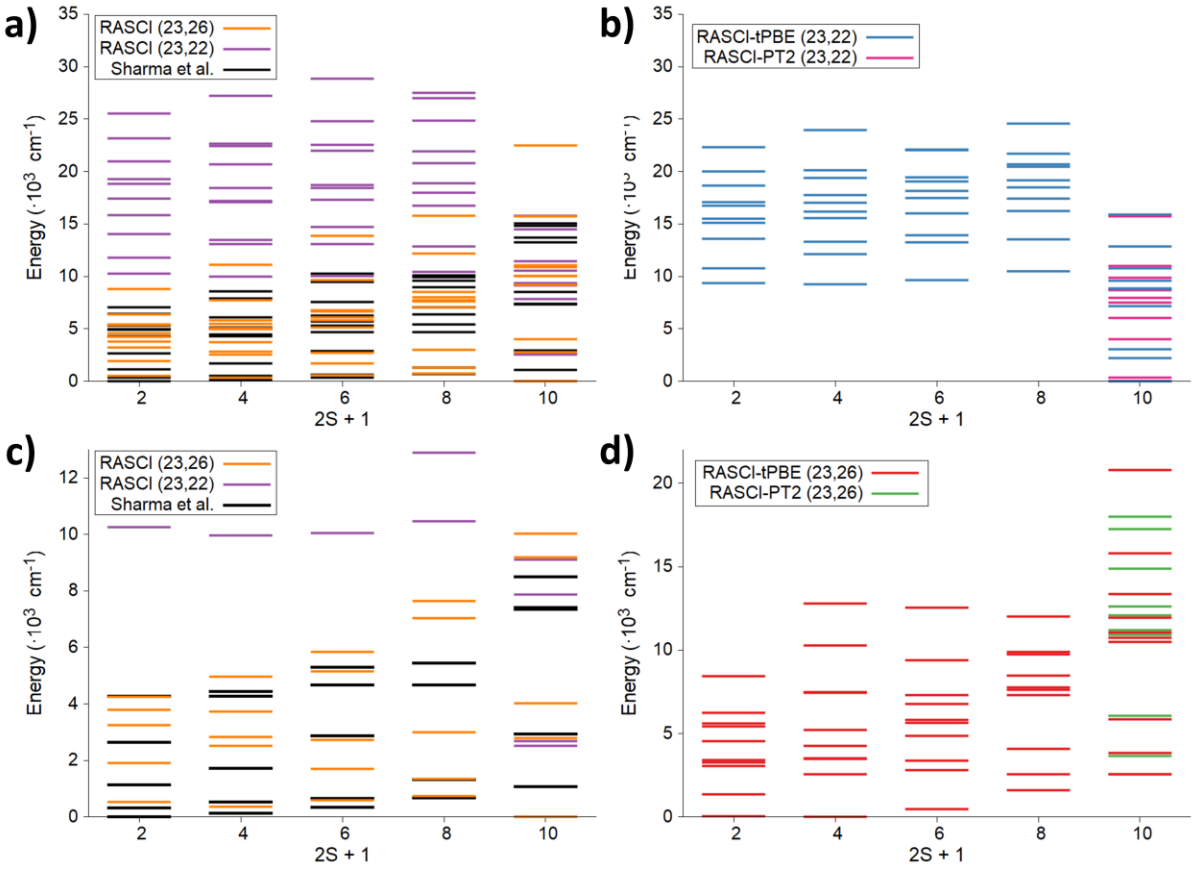

Figure 3. (a) RASCI spin ladder for the unrelaxed $[Fe_2S_2(SCH_3)_4]^{3-}$ cluster, computed with the two active spaces. The DMRG-CASCI results of Sharma et al.[16] are also shown. (b) RASCI-PDFT spin ladder and RASCI-PT2 dectet results with the (23,22) active space. Panel (c) shows a closer view than (a) on the lowest five states for the RASCI (23,26) and the DMRG-CASCI data. (d) RASCI-PDFT spin ladder and RASCI-PT2 dectet results with the (23,26) active space. The doublet ground state is taken as zero. As in Figure 2, the RASPT2 energies of panel (d) are shifted to the RASCI-tPBE dectet ground state. In the figure, RASCI-PDFT is labeled RASCI-tPBE.

3.2.2 Reduced cluster with relaxed geometry

Table 4 reports the lowest vertical excitation energies of the relaxed reduced cluster (full data is available in Table S4). In contrast to the results for the unrelaxed cluster, the (23,21) active space RASCI results are much closer to those of the (23,26) active space and to those obtained by DMRG-CASCI for low-energy states, although there are very large differences for higher-energy states (see Table S4 and Figure S5). There is also one fewer 3*d*´ orbital in the (23,21) active space than in the corresponding unrelaxed case (23,22) due to its very small occupation (0.01). However, the inclusion of all correlating *3d*´ orbitals in the (23,26) active space makes a remarkable improvement in the description of the internal correlation contribution to higher excitation energies. Energy levels corresponding to Table 4 are shown in Figure S5b.

Table 4 RASCI vertical excitation energies for the lowest five electronic states with respect to the DMRG-CASCI results of Sharma et al.[16] for the relaxed geometry of the reduced cluster. The lowest energies in each case are set to zero.

	Excitation energies (eV)									
	RASCI (23,1,1;6,10,10)					**RASCI (23,1,1;6,10,5)**				
2S+1	**State 1**	**State 2**	**State 3**	**State 4**	**State 5**	**State 1**	**State 2**	**State 3**	**State 4**	**State 5**
2	0.04	0.15	0.38	0.42	0.50	0.00	0.12	0.35	0.38	0.46
4	0.05	0.15	0.37	0.42	0.51	0.01	0.13	0.36	0.39	0.47
6	0.04	0.15	0.37	0.41	0.55	0.03	0.15	0.37	0.42	0.50
8	0.02	0.18	0.38	0.44	0.61	0.04	0.19	0.40	0.46	0.56

10	0.00	0.23	0.40	0.50	0.69	0.04	0.24	0.46	0.51	0.64
	DMRG-CASCI, Sharma et al.[16]									
	State 1	**State 2**	**State 3**	**State 4**	**State 5**					
2	0.00	0.15	0.26	0.47	0.50					
4	0.03	0.15	0.29	0.52	0.56					
6	0.08	0.16	0.35	0.57	0.61					
8	0.10	0.17	0.42	0.64	0.67					
10	0.12	0.23	0.53	0.74	0.80					

For the relaxed reduced cluster, for which the relative energies are depicted in Figures 4a and 4b, the most notable difference from the unrelaxed cluster is that RASCI-PDFT predicts the ground state of the spin ladder to be the dectet (ferromagnetic) spin configuration in both active spaces. This is also in contrast with previous DMRG-CASCI calculations[16] for both unrelaxed and relaxed structures. This dectet ground state is compatible with some experimental observations of a high-spin ground state in valence-delocalized [2Fe-2S] reduced clusters,[58–60] where the two iron centers are $Fe^{+2.5}$. The reversed stability is not evident at the RASCI level (see Figure S5 as compared to Figure 4), which suggests that a beyond-MCSCF treatment (i.e., inclusion of external correlation energy) is necessary. Such a treatment was absent in the DMRG-CASCI calculations of Ref. 16. The experimental cases very often feature a low-spin ground state, but more generally there may be a strong dependence on geometry (see also Section 3.3). Thus, no general statements can be made about the ground spin of all [2Fe-2S] clusters. Regardless, our results give evidence to the potentially dramatic effects of including (or, conversely, ignoring) dynamic correlation.

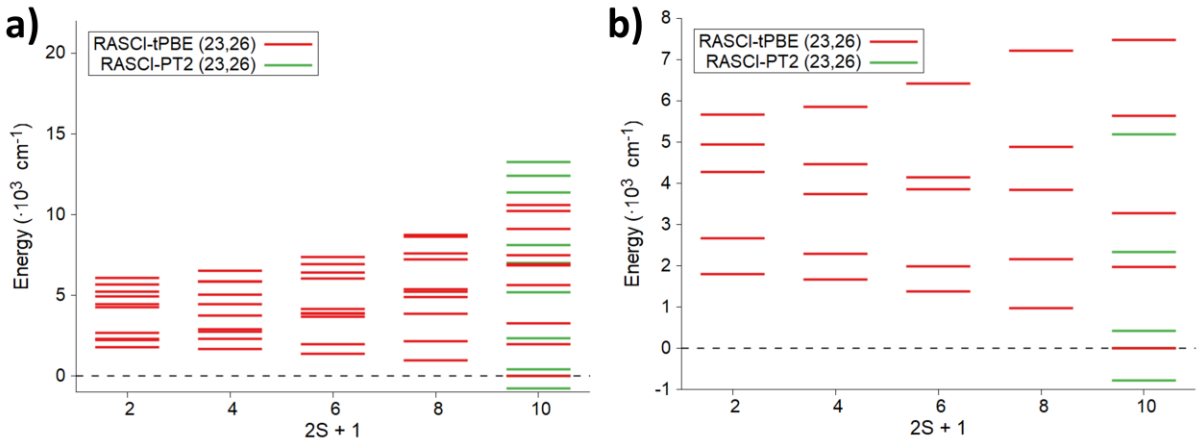

Figure 4. (a) RASCI-PDFT spin ladder for the relaxed $[Fe_2S_2(SCH_3)_4]^{3-}$ cluster, computed with the large active space. The RASCI-PT2 dectet results are also shown. The RASCI-PT2 energies are shifted to the RASCI-PDFT dectet ground state, which is taken as the zero of energy. In the figure, RASCI-PDFT is labeled RASCI-tPBE. (b) A closer look at the lower-energy states of panel (a) (note that for the highest-spin case, the RASCI-tPBE and RASCI-PT2 states at 0.00 eV are superimposed).

RASCI-PT2 calculations either did not converge or were not feasible except for the dectet. The corresponding energy values (reported in Tables S2-S4) are shown in Figure 4. Note that Figure 4 shows what appears to be a negative excitation energy. This is because the RASCI-PT2 states are not ordered the same as RASCI and RASCI-PDFT. Using the labeling scheme in Table S4, the "State 1" dectet is the ground state at the RASCI and RASCI-PDFT levels. To make comparison of relative energies easier, the RASCI-PT2 energies are shifted so that the energy of State 1 is zero. However, the State 2 RASCI-PT2 energy is lower than the State 1 RASCI-PT2 energy and so appears to be negative after the shift (see also Table S4).

3.3 Configurations and populations

Looking at the main electronic configurations of the lowest energy high-spin states (Table S5), we note that the dominant configurations in all systems have weights (squared CI coefficients) far from unity. This means that the corresponding wave functions have significant multi-configurational character.

The lowest-energy undectet (high) spin state of the oxidized cluster has three contributions with weight greater than 0.10, with one clearly dominant but having a relatively small weight (0.53). This is also seen for the lowest-energy dectet state of the reduced cluster at the same (unrelaxed) geometry (weight: 0.62). In contrast, the weight of the dominant configuration for the lowest-energy dectet state at the relaxed geometry is only 0.21 and is accompanied by three other high-spin configurations that have similar weights (0.12, 0.16, and 0.11). The state-specific configurations (Table S5) also show a slightly diminished occupancy of 3*p* orbitals of the bridging sulfurs. The spin densities reported in Tables S6-S8 of the SI show that in the high-spin cases one of the unpaired electrons is delocalized over the bridging sulfurs for the oxidized cluster, whereas for the two reduced clusters it is delocalized over the entire [2Fe-2S] fragment. The reduced cluster shows a nearly symmetric electronic structure at the unrelaxed geometry and a slightly asymmetric structure at the relaxed geometry.

Formally the oxidation states for the oxidized and reduced clusters are Fe^{+3}/Fe^{+3} and Fe^{+3}/Fe^{+2}, respectively, but the orbital occupation numbers in the ground states (see Figures S6-S8) suggest the reduced cluster is better described as $Fe^{+2.5}/Fe^{+2.5}$, which is in agreement with some experimental conclusions.[58–60] The additional electron in the reduced cluster as compared to the oxidized cluster is found in a bonding/antibonding pair of 3*d* orbitals and is evenly distributed over the two Fe centers. At the unrelaxed geometry it appears almost entirely in the δ/δ* combination of the Fe $3d_{yz}$ orbitals, with the additional occupancy being added evenly between the δ and δ* orbitals. In contrast, at the relaxed geometry it is in the σ bonding combination of the Fe $3d_{z^2}$ orbitals, and with the σ* antibonding orbital being less occupied than in the oxidized case or in the reduced unrelaxed cluster. These observations may be explained by the relaxed geometry having an Fe-Fe distance of 2.91 Å, which is longer than 2.69 Å of the unrelaxed geometry; the greater distance correlates with the more favorable σ-bonding interaction.

4. Conclusions

We have shown that RASCI-PDFT is an affordable way to approximate the full electron correlation in systems like [2Fe-2S] clusters that require multireference wave functions containing a large

number of orbitals in the active space (26) and a large number of a configuration state functions (over six million). Our results with RASCI-PDFT show that correlation effects beyond those included in CASSCF, RASSCF, CASCI, and RASCI, even with the large active spaces allowed by DMRG solvers, can be considerable in these systems. These correlation effects cannot currently be evaluated by standard post-MCSCF methods such as RASCI-PT2, which remains unaffordable for most of the low-spin multiplets.

Both oxidized and reduced clusters at their unrelaxed geometry have a low-spin ground state. However, in contrast with previous calculations, a reversed spin-ladder energy ordering is obtained with RASCI-PDFT for the reduced [2Fe-2S] cluster at the relaxed geometry. This is in agreement with some previous experimental observations of a high-spin ground state in valence-delocalized [2Fe-2S] clusters.

RASCI-PDFT makes the treatment of full correlation with bimetallic systems affordable, as demonstrated by the calculation of full spin ladders where only the highest-spin cases were feasible with RASPT2. A suitable improvement over RASCI-PDFT, and a good compromise between accuracy and feasibility towards larger active spaces and compounds, would be the use of the recently developed DMRG-PDFT[61] method. The combination of DMRG's powerful ability to reduce the number of configurations in a large active space with MC-PDFT's evaluation of the full electron correlation will allow a quantitative description of larger iron-sulfur clusters, e.g. [4Fe-4S], as well as an unprecedented possibility to investigate very large systems with a fully multi-configurational approach.

■ ASSOCIATED CONTENT

Supporting Information

The Supporting Information is available free of charge on the ACS Publications website at DOI: 10.1021/

Orbitals and active spaces, detailed active space search protocol, vertical excitation energies and spin ladders, RASCI dominant configurations, partial atomic charges and spin populations, structures, SA-RASCI absolute energies. (PDF) RASCI optimized state-average natural orbitals in the Molcas format (RasOrb, plaint text). (ZIP archive)

AUTHOR INFORMATION

Corresponding Authors
*E-mail: truhlar@umn.edu; gagliard@umn.edu

ORCID
Davide Presti: 0000-0002-7836-1442
Samuel J. Stoneburner: 0000-0001-8394-0572
Donald G. Truhlar: 0000-0002-7742-7294
Laura Gagliardi: 0000-0001-5227-1396

Notes
The authors declare no competing financial interest.

ACKNOWLEDGMENT

We thank C. A. Gaggioli for helpful discussions. This work was supported in part by the National Science Foundation by grant no. CHE-1464536.

REFERENCES

(1) Beinert, H.; Holm, R. H.; Münck, E. Iron-Sulfur Clusters: Nature's Modular, Multipurpose Structures. *Science* **1997**, *277*, 653–659.

(2) Österberg, R. Origins of Metal Ions in Biology. *Nature* **1974**, *249*, 382–383.

(3) Gillum, W. O.; Frankel, R. B.; Foner, S.; Holm, R. H. Synthetic Analogues of the Active Sites of Iron-Sulfur Proteins. XIII. Further Electronic Structural Relationships between the Analogues [Fe2S2(SR)4]2- and the Active Sites of Oxidized 2Fe-2S* Proteins. *Inorg. Chem.* **1976**, *15*, 1095–1100.

(4) Scintilla, S.; Bonfio, C.; Belmonte, L.; Forlin, M.; Rossetto, D.; Li, J.; A. Cowan, J.; Galliani, A.; Arnesano, F.; Assfalg, M.; et al. Duplications of an Iron–sulphur Tripeptide Leads to the Formation of a Protoferredoxin. *Chem. Commun.* **2016**, *52*, 13456–13459.

(5) Qi, W.; Cowan, J. A. Structural, Mechanistic and Coordination Chemistry of Relevance to the Biosynthesis of Iron–sulfur and Related Iron Cofactors. *Coord. Chem. Rev.* **2011**, *255*, 688–699.

(6) Blondin, G.; Girerd, J. J. Interplay of Electron Exchange and Electron Transfer in Metal Polynuclear Complexes in Proteins or Chemical Models. *Chem. Rev.* **1990**, *90*, 1359–1376.

(7) Dutta, S. K.; Ensling, J.; Werner, R.; Flörke, U.; Haase, W.; Gütlich, P.; Nag, K. Valence-Delocalized and Valence-Trapped FeIIFeIII Complexes: Drastic Influence of the Ligands. *Angew. Chemie Int. Ed. English* **1997**, *36*, 152–155.

(8) Wächtershäuser, G. Groundworks for an Evolutionary Biochemistry: The Iron-Sulphur World. *Prog. Biophys. Mol. Biol.* **1992**, *58*, 85–201.

(9) Wächtershäuser, G. Life as We Don't Know It. *Science (80-.).* **2000**, *289*, 1307–1308.

(10) Wächtershäuser, G. Before Enzymes and Templates: Theory of Surface Metabolism. *Microbiol. Rev.* **1988**, *52*, 452–484.

(11) Wächtershäuser, G. Evolution of the First Metabolic Cycles. *Proc. Natl. Acad. Sci.* **1990**, *87*, 200–204.

(12) Bonfio, C.; Valer, L.; Scintilla, S.; Shah, S.; Evans, D. J.; Jin, L.; Szostak, J. W.; Sasselov, D. D.; Sutherland, J. D.; Mansy, S. S. UV-Light-Driven Prebiotic Synthesis of Iron–sulfur Clusters. *Nat. Chem.* **2017**, *9*, 1229–1234.

(13) Venkateswara Rao, P.; Holm, R. H. Synthetic Analogues of the Active Sites of Iron—Sulfur Proteins. *Chem. Rev.* **2004**, *104*, 527–560.

(14) Pandelia, M.-E.; Lanz, N. D.; Booker, S. J.; Krebs, C. Mössbauer Spectroscopy of Fe/S Proteins. *Biochim. Biophys. Acta - Mol. Cell Res.* **2015**, *1853*, 1395–1405.

(15) Koch, F.; Berkefeld, A.; Speiser, B.; Schubert, H. Mechanistic Aspects of Redox-Induced Assembly and Disassembly of S-Bridged [2M-2S] Structures. *Chem. – A Eur. J.* **2017**, *23*, 16681–16690.

(16) Sharma, S.; Sivalingam, K.; Neese, F.; Chan, G. K. L. Low-Energy Spectrum of Iron-Sulfur Clusters Directly from Many-Particle Quantum Mechanics. *Nat. Chem.* **2014**, *6*, 927–933.

(17) Noodleman, L.; Davidson, E. R. Ligand Spin Polarization and Antiferromagnetic Coupling in Transition Metal Dimers. *Chem. Phys.* **1986**, *109*, 131–143.

(18) Noodleman, L.; Peng, C. Y.; Case, D. A.; Mouesca, J.-M. Orbital Interactions, Electron Delocalization and Spin Coupling in Iron-Sulfur Clusters. *Coord. Chem. Rev.* **1995**, *144*, 199–244.

(19) Ruiz, E.; Cano, J.; Alvarez, S.; Alemany, P. Broken Symmetry Approach to Calculation of Exchange Coupling Constants for Homobinuclear and Heterobinuclear Transition Metal Complexes. *J. Comput. Chem.* **1999**, *20*, 1391–1400.

(20) Raghu, C.; Rudra, I.; Sen, D.; Ramasesha, S. Properties of Low-Lying States in Some High-Nuclearity Mn, Fe, and V Clusters: Exact Studies of Heisenberg Models. *Phys. Rev. B* **2001**, *64*, 64419.

(21) Hübner, O.; Sauer, J. Structure and Thermochemistry of Fe2S2−/0/+ Gas Phase Clusters and Their Fragments. B3LYP Calculations. *Phys. Chem. Chem. Phys.* **2002**, *4*, 5234–5243.

(22) Hübner, O.; Sauer, J. The Electronic States of Fe2S2−/0/+/2+. *J. Chem. Phys.* **2001**, *116*, 617–628.

(23) Shoji, M.; Koizumi, K.; Taniguchi, T.; Kitagawa, Y.; Yamanaka, S.; Okumura, M.; Yamaguchi, K. Theory of Chemical Bonds in Metalloenzymes III: Full Geometry Optimization and Vibration Analysis of Ferredoxin-Type [2Fe–2S] Cluster. *Int. J. Quantum Chem.* **2007**, *107*, 116–133.

(24) Chang, C. H.; Kim, K. Density Functional Theory Calculation of Bonding and Charge Parameters for Molecular Dynamics Studies on [FeFe] Hydrogenases. *J. Chem. Theory Comput.* **2009**, *5*, 1137–1145.

(25) Li, Z.; Chan, G. K.-L. Spin-Projected Matrix Product States: Versatile Tool for Strongly Correlated Systems. *J. Chem. Theory Comput.* **2017**, *13*, 2681–2695.

(26) Dong, G.; Phung, Q. M.; Hallaert, S. D.; Pierloot, K.; Ryde, U. H2 Binding to the Active Site of [NiFe] Hydrogenase Studied by Multiconfigurational and Coupled-Cluster Methods. *Phys. Chem. Chem. Phys.* **2017**, *19*, 10590–10601.

(27) Chu, S.; Bovi, D.; Cappelluti, F.; Orellana, A. G.; Martin, H.; Guidoni, L. Effects of Static Correlation between Spin Centers in Multicenter Transition Metal Complexes. *J. Chem. Theory Comput.* **2017**, *13*, 4675–4683.

(28) Barborini, M.; Guidoni, L. Geometries of Low Spin States of Multi-Centre Transition Metal Complexes through Extended Broken Symmetry Variational Monte Carlo. *J. Chem. Phys.* **2016**, *145*, 124107.

(29) Roos, B. O.; Taylor, P. R.; Siegbahn, P. E. M. A Complete Active Space SCF Method (CASSCF) Using a Density

Matrix Formulated Super-CI Approach. *Chem. Phys.* **1980**, *48*, 157–173.

(30) Werner, H.; Knowles, P. J. An Efficient Internally Contracted Multiconfiguration–reference Configuration Interaction Method. *J. Chem. Phys.* **1988**, *89*, 5803–5814.

(31) Andersson, K.; Malmqvist, P. A.; Roos, B. O.; Sadlej, A. J.; Wolinski, K. Second-Order Perturbation Theory with a CASSCF Reference Function. **1990**, *94*, 5483–5488.

(32) Andersson, K.; Malmqvist, P.; Roos, B. O. Second-order Perturbation Theory with a Complete Active Space Self-consistent Field Reference Function. *J. Chem. Phys.* **1992**, *96*, 1218–1226.

(33) Malmqvist, P. Å.; Pierloot, K.; Shahi, A. R. M.; Cramer, C. J.; Gagliardi, L. The Restricted Active Space Followed by Second-Order Perturbation Theory Method: Theory and Application to the Study of CuO2 and Cu2O2 Systems. *J. Chem. Phys.* **2008**, *128*, 204109.

(34) Li Manni, G.; Carlson, R. K.; Luo, S.; Ma, D.; Olsen, J.; Truhlar, D. G.; Gagliardi, L. Multiconfiguration Pair-Density Functional Theory. *J. Chem. Theory Comput.* **2014**, *10*, 3669–3680.

(35) Ghosh, S.; Sonnenberger, A. L.; Hoyer, C. E.; Truhlar, D. G.; Gagliardi, L. Multiconfiguration Pair-Density Functional Theory Outperforms Kohn–Sham Density Functional Theory and Multireference Perturbation Theory for Ground-State and Excited-State Charge Transfer. *J. Chem. Theory Comput.* **2015**, *11*, 3643–3649.

(36) Carlson, R. K.; Truhlar, D. G.; Gagliardi, L. Multiconfiguration Pair-Density Functional Theory: A Fully Translated Gradient Approximation and Its Performance for Transition Metal Dimers and the Spectroscopy of Re2Cl82–. *J. Chem. Theory Comput.* **2015**, *11*, 4077–4085.

(37) Sharma, P.; Truhlar, D. G.; Gagliardi, L. Active Space Dependence in Multiconfiguration Pair-Density Functional Theory. *J. Chem. Theory Comput.* **2018**, *14*, 660–669.

(38) Ghosh, S.; Verma, P.; Cramer, C. J.; Gagliardi, L.; Truhlar, D. G. Combining Wave Function Methods with Density Functional Theory for Excited States. *Chem. Rev.* **2018**, *118*, 7249–7292.

(39) Presti, D.; Truhlar, D. G.; Gagliardi, L. Intramolecular Charge Transfer and Local Excitation in Organic Fluorescent Photoredox Catalysts Explained by RASCI-PDFT. *J. Phys. Chem. C* **2018**, *122*, 12061–12070.

(40) Malmqvist, P. A.; Rendell, A.; Roos, B. O. The Restricted Active Space Self-Consistent-Field Method, Implemented with a Split Graph Unitary Group Approach. *J. Phys. Chem.* **1990**, *94*, 5477–5482.

(41) Olsen, J.; Roos, B. O.; Jo/rgensen, P.; Jensen, H. J. A. Determinant Based Configuration Interaction Algorithms for Complete and Restricted Configuration Interaction Spaces. *J. Chem. Phys.* **1988**, *89*, 2185–2192.

(42) Sauri, V.; Serrano-Andrés, L.; Shahi, A. R. M.; Gagliardi, L.; Vancoillie, S.; Pierloot, K. Multiconfigurational Second-Order Perturbation Theory Restricted Active Space (RASPT2) Method for Electronic Excited States: A Benchmark Study. *J. Chem. Theory Comput.* **2011**, *7*, 153–168.

(43) Aquilante, F.; Autschbach, J.; Carlson, R. K.; Chibotaru, L. F.; Delcey, M. G.; De Vico, L.; Fdez. Galván, I.; Ferré, N.; Frutos, L. M.; Gagliardi, L.; et al. Molcas 8: New Capabilities for Multiconfigurational Quantum Chemical Calculations across the Periodic Table. *J. Comput. Chem.* **2016**, *37*, 506–541.

(44) Widmark, P.-O.; Malmqvist, P.-Å.; Roos, B. O. Density Matrix Averaged Atomic Natural Orbital (ANO) Basis Sets for Correlated Molecular Wave Functions. *Theor. Chim. Acta* **1990**, *77*, 291–306.

(45) Douglas, M.; Kroll, N. M. Quantum Electrodynamical Corrections to the Fine Structure of Helium. *Ann. Phys. (N. Y).* **1974**, *82*, 89–155.

(46) Hess, B. A. Relativistic Electronic-Structure Calculations Employing a Two-Component No-Pair Formalism with External-Field Projection Operators. *Phys. Rev. A* **1986**, *33*, 3742–3748.

(47) Wolf, A.; Reiher, M.; Hess, B. A. The Generalized Douglas–Kroll Transformation. *J. Chem. Phys.* **2002**, *117*, 9215–9226.

(48) Stålring, J.; Bernhardssonn, A.; Lindh, R. Analytical Gradients of a State Average MCSCF State and a State Average Diagnostic. *Mol. Phys.* **2001**, *99*, 103–114.

(49) Forsberg, N.; Malmqvist, P.-Å. Multiconfiguration Perturbation Theory with Imaginary Level Shift. *Chem. Phys. Lett.* **1997**, *274*, 196–204.

(50) Ghigo, G.; Roos, B. O.; Malmqvist, P.-Å. A Modified Definition of the Zeroth-Order Hamiltonian in Multiconfigurational Perturbation Theory (CASPT2). *Chem. Phys. Lett.* **2004**, *396*, 142–149.

(51) Gagliardi, L.; Truhlar, D. G.; Li Manni, G.; Carlson, R. K.; Hoyer, C. E.; Bao, J. L. Multiconfiguration Pair-Density Functional Theory: A New Way To Treat Strongly Correlated Systems. *Acc. Chem. Res.* **2017**, *50*, 66–73.

(52) Kovačević, G.; Veryazov, V. Luscus: Molecular Viewer and Editor for MOLCAS. *J. Cheminform.* **2015**, *7*, 16.

(53) Momma, K.; Izumi, F. VESTA 3 for Three-Dimensional Visualization of Crystal, Volumetric and Morphology Data. *J. Appl. Crystallogr.* **2011**, *44*, 1272–1276.

(54) Mayerle, J. J.; Denmark, S. E.; DePamphilis, B. V; Ibers, J. A.; Holm, R. H. Synthetic Analogs of the Active Sites of Iron-Sulfur Proteins. XI. Synthesis and Properties of Complexes Containing the Iron Sulfide (Fe2S2) Core and the Structures of Bis[o-Xylyl-.Alpha.,.Alpha.'-Dithiolato-.Mu.-Sulfido-Ferrate(III)] and Bis[p-Tolylthiol. *J. Am. Chem. Soc.* **1975**, *97*, 1032–1045.

(55) Ghosh, S.; J. Cramer, C.; G. Truhlar, D.; Gagliardi, L. Generalized-Active-Space Pair-Density Functional Theory: An Efficient Method to Study Large, Strongly Correlated, Conjugated Systems. *Chem. Sci.* **2017**, *8*, 2741–2750.

(56) Pierloot, K. Nondynamic Correlation Effects in Transition Metal Coordination Compounds. In *Computational Organometallic Chemistry*; Cundari, T. R. Ed.; Marcel Dekker: New York, 2001; pp 123–158.

(57) Stoneburner, S. J.; Gagliardi, L. Air Separation by Catechol-Ligated Transition Metals: A Quantum Chemical Screening. *J. Phys. Chem. C* **2018**, *122*, 22345–22351.

(58) Crouse, B. R.; Meyer, J.; Johnson, M. K. Spectroscopic Evidence for a Reduced Fe2S2 Cluster with a S = 9/2 Ground State in Mutant Forms of Clostridium Pasteurianum 2Fe Ferredoxin. *J. Am. Chem. Soc.* **1995**, *117*, 9612–9613.

(59) Achim, C.; Golinelli, M.-P.; Bominaar, E. L.; Meyer, J.; Münck, E. Mössbauer Study of Cys56Ser Mutant 2Fe Ferredoxin from Clostridium Pasteurianum: Evidence for Double Exchange in an [Fe2S2]+ Cluster. *J. Am. Chem. Soc.* **1996**, *118*, 8168–8169.

(60) Subramanian, S.; Duin, E. C.; Fawcett, S. E. J.; Armstrong, F. A.; Meyer, J.; Johnson, M. K. Spectroscopic and Redox Studies of Valence-Delocalized [Fe2S2]+ Centers in Thioredoxin-like Ferredoxins. *J. Am. Chem. Soc.* **2015**, *137*, 4567–4580.

(61) Sharma, P.; Bernales, V.; Knecht, S.; Truhlar, D. G.; Gagliardi, L. Density Matrix Renormalization Group Pair-Density Functional Theory (DMRG-PDFT): Singlet-Triplet Gaps in Polyacenes and Polyacetylenes. *Chem. Sci.* **2019**, *10*, 1716–1723.

TOC Graphics